An observational study of cometary globules near the Rosette nebula

Journal Item

Astron. Astrophys. 323, 931–942 (1997)

ASTRONOMY
AND
ASTROPHYSICS

An observational study of cometary globules near the Rosette nebula

Glenn J. White[1], B. Lefloch[2], C.V.M. Fridlund[3], C.A. Aspin[4], G. Dahmen[1], N.R. Minchin[1], and M. Huldtgren[5]

[1] Department of Physics, Queen Mary and Westfield College, University of London, Mile End Road, London E1 4NS, UK
[2] IRAM, 300 Rue de la Piscine, F-38406 St Martin d'Hères, France
[3] ESA Astrophysics Division, Space Science Department, ESTEC, P.O. Box 299, 2200 AG Noordwijk, The Netherlands
[4] Joint Astronomy Centre, 660 N A'ohoku, University Park, Hilo, Hawaii, USA
[5] Stockholm Observatory, S-133 36 Saltsjöbaden, Sweden

Received 26 June 1996 / Accepted 20 November 1996

Abstract. Molecular line observations are reported of two regions containing small cometary globules at the edge of the Rosette Nebula. Observations of the CO, ^{13}CO and C^{18}O $J = 2 - 1$, and CO $J = 4 - 3$ molecular lines towards Globule 1, the most prominent of the group, show it has a well-developed head-tail structure, with a head diameter ~ 0.4 pc, and a tail extending ~ 1.3 pc behind it. The major axis of the system points about 45 degrees away from the direction to the centre of the Rosette Nebula (which contains the [presumed] illuminating stars), and 20 degrees out of the plane of the sky, along a projected line towards the luminous (924 $L_\odot$) infrared source IRAS 06314+0427. The CO lines have a complex velocity structure; with a pronounced broadening at the front of the head (as viewed from IRAS 06314+0427); a velocity gradient ~ 1.4 km s^{-1} along the tail, and material at the front of the head is blue-shifted by ~ 0.5 km s^{-1} compared to surrounding gas. The CO $J = 2 - 1$ line intensity peaks towards the front of the head, and along the edges of the tail. The ^{13}CO $J = 2 - 1$ antenna temperatures in the head are very similar to those of CO, suggesting very high opacities or column densities, or that there is significant CO self-absorption. There is a narrow rim of CO $J = 4 - 3$ emission around the front of the head over a limited velocity range, which correlates with the position of a faint optical rim, and a narrow ridge of 2 μm H_2 emission. These data give strong support to the Radiation Driven Implosion (RDI) model of Lefloch and Lazareff (1994 — hereafter LL94), which was developed to explain the physical structure of cometary globules. Using an RDI simulation, a remarkably good fit to the data has been obtained, allowing the CO, ^{13}CO and C^{18}O spatial structures and velocity field to be modelled. This simulation suggests that Globule 1 is $\sim 400{,}000$ years old, and has a mass ~ 50 $M_\odot$. Additional observations towards the region close to IRAS 06314+0427 show that it is associated with an intense molecular concentration lying at the northern end of a ~ 5 pc long molecular ridge, with a mass ~ 330 $M_\odot$, and lies close to the centre of a shell-like condensation.

Key words: stars: formation – ISM: Rosette nebula – shocks – ISM: molecules – radio lines: ISM

1. Introduction

Cometary globules are small, low mass molecular clouds, recognisable by their distinctive head-tail, core-halo or 'cometary' appearance (Hawarden & Brand 1976). A survey of IRAS point sources with far-infrared colours typical of pre-main sequence objects and a series of targeted molecular line studies, found several which were associated with cometary globules, suggesting that some of them contain active regions of star formation (Sugitani et al.1991; Reipurth 1983; White 1994; González-Alfonso et al.1995). It is likely that the star formation activity in these objects has followed the Radiation Driven Implosion of a parental cloud which is illuminated by the ultraviolet radiation of nearby OB stars (Sanford et al.1982). In this paper millimetre, submillimetre, optical and near-infrared wavelength observations are reported of a region containing several small cometary globules at the south-eastern edge of the Rosette Nebula.

In a recent CO $J = 1-0$ survey of an 0.25 square degree area at the edge of the Rosette Nebula H II region (NGC 2237-2246, distance ~ 1.6 kpc, for which 1 arc second correponds to a linear size of ~ 0.008 pc), Patel et al.(1993) identified nine molecular clumps which they referred to as 'globules' — small molecular clouds with masses in the range $50 - 300$ $M_\odot$, diameters of 0.7 to 2.3 parsecs and temperatures in the range $10 - 16$ K. Globule 1, visually the most prominent, has a faint optical rim, which can be seen clearly (with contrast enhancement) on the red Palomar Sky Survey (POSS) plate. This rim lies along the north-western edge of the globule that is illuminated by the five O stars (~ 28 pc to the north-west of the globule's head) which dominate the ionisation of the Rosette Nebula. These stars have a total luminosity $\sim 1.1\ 10^6$ $L_\odot$, emit $\sim 1\ 10^{50}$ ionising

Send offprint requests to: Prof Glenn White

Table 1. Telescope and receiver characteristics

Line	Transition	Freq GHz	HPBW $''$	$\eta_{\rm mb}$	$\eta_{\rm fss}$	System Noise Temperature K	rms K	No of spectra	Telescope
^{13}CO	$J = 1 - 0$	110.201	34	0.52	0.73	200	0.15	1	OSO
CO	$J = 1 - 0$	115.271	33	0.52	0.73	200	0.15	1	OSO
C^{18}O	$J = 2 - 1$	219.560	20	0.63	0.77	330	0.4	54	JCMT
^{13}CO	$J = 2 - 1$	220.398	19	0.63	0.77	360	0.4	112	JCMT
CO	$J = 2 - 1$	230.538	19	0.63	0.77	370	0.3	106	JCMT
CO	$J = 4 - 3$	461.041	11	0.48	0.68	2300	1.9	49	JCMT
CI	$^3P_1 - {}^3P_0$	492.160	10	0.46	0.67	3100	1.1	1	JCMT

photons s^{-1} (Dorland et al.1986; Cox et al.1990; Bertoldi & McKee 1990), and provide a flux of ionising photons at the surface of the globule of $\leqq$ 1.1 10^9 cm^{-2} s^{-1} — similar to values inferred towards several other cometary globules (LL94, Lefloch & Lazareff, 1995 (hereafter LL95)).

Observations of Globule 1 have been reported at optical and far-infrared wavelengths, and millimetre wave spectral line data have been used to probe the properties of the molecular gas (Block 1990; Sugitani et al.1991; Patel et al.1993). Globule 1 contains an infrared source, IRAS 06322+0427 (L_{IRAS} = 131 $L_\odot$), and lies close to several other IRAS sources (06314+0427 (924 $L_\odot$), 06314+0421 (737 $L_\odot$), 06318+0420 (1368 $L_\odot$) and 06319+0415 (7622 $L_\odot$ - also known as AFGL 961)). The major axis of the head-tail system of Globule 1 points towards IRAS 06314+0427, which has been suggested to be either an embedded O7 star, or a cluster of less massive stars (Block 1990; Block et al.1992; Patel et al.1993). The ionising flux rate of a single O7 star is $\sim$ 2 10^{48} s^{-1}; at a projected distance from Globule 1 of $\sim$ 5 pc, this would provide an ionising flux at the surface of Globule 1 of 7.1 10^8 cm^{-2} s^{-1}, in the absence of significant line of sight extinction. If however, as Block et al.(1992) suggest, IRAS 06314+0427 contains a cluster of less massive stars, their ionising flux at the surface of Globule 1 is likely to be insignificant in comparison with the flux due to the Rosette Nebula's OB stars. The fact that the axis of Globule 1 points towards IRAS 06314+0427 suggests that it may have had some effect on the globule's evolution. Since the $J = 1 - 0$ mapping by Patel et al.(1993), the increased spatial resolution available from the JCMT observations ($10 - 21$ arc second beam compared to the $J = 1 - 0$ FCRAO study: 44 arc second beam), and improved theoretical modelling techniques have made it worthwhile to obtain high quality data in an attempt to better constrain the structure and physical conditions inside the globule.

2. The observations

The CO *J*= 2-1 and 4-3 data, and a spectrum in the $^3P_1$ – $^3P_0$ atomic carbon fine structure line were obtained with the 15 metre James Clerk Maxwell Telescope (JCMT) in Hawaii during October 1994 and November 1995. These observations were made during good atmospheric conditions, with the pointing and tracking accuracy better than 2 arc seconds. The CO and C I observations were made with position switching to a clean off position, whilst the ^{13}CO and C^{18}O observations were obtained using frequency switching at the same time as fast raster grid mapping. The data were collected and processed using SIS receivers and a digital autocorrelation spectrometer backend (White 1988; Ellison et al.1995), to achieve velocity resolutions $\sim$ 0.1 km s^{-1} . The observing parameters for the molecular line observations are summarised in Table 1. The data were calibrated in units of main beam brightness temperature $T_{\rm mb}$ or corrected antenna temperature $T_{\rm r}{}^*$, using a standard chopper wheel calibration technique. Despite very careful attempts at accurate calibration, we estimate the absolute uncertainty of the $J = 2 - 1$ data is no better than 12 %. The telescope efficiencies were estimated from observations of the Moon, Jupiter and Mars, and are believed to be good to 15 %. The efficiencies at 461 and 492 GHz have an absolute uncertainty no better than 20 %. In general $T_{\rm mb}$ has been used throughout this paper since much of the emission is contained in small clumpy structures — except for the CO maps, where the $T_{\rm r}{}^*$ is used, as this provides a more realistic estimator of the CO kinetic temperature. Several CO and ^{13}CO $J = 1 - 0$ spectra were obtained during April 1995 with the Onsala Space Observatory 20 metre telescope, using an SIS receiver with a 256 x 250 kHz filter bank operated in a position switching mode.

The near-infrared data were collected using the infrared camera IRCAM3 on the 3.8 metre United Kingdom Infrared Telescope (UKIRT), with a 1 percent bandwidth filter centred at the H_2 $v = 1 - 0$ S(1) wavelength (2.122 μm) with a pixel size and seeing disc of 0.286 and 0.72 arc seconds respectively. The observations were flat-fielded and calibrated against nearby standard stars. A broadband K image was also taken of the field, but due to seeing fluctuations throughout the exposure, was not considered to be reliable enough to subtract the continuum emission. This K image did however show all of the stars seen in the 2.122 μm frame, but contained none of the extended H_2 emission which will be shown later in Fig. 11a.

The H_α images were obtained using the Nordic Optical Telescope (NOT) at La Palma in January 1996, as part of a spectrophotometric imaging survey of cometary globules, which will be reported elsewhere. For the data shown in this paper, a 1K x 1K backside illuminated thinned Tektronix CCD chip with 0.176 arc second pixels was used with a narrow-band (3 nm)

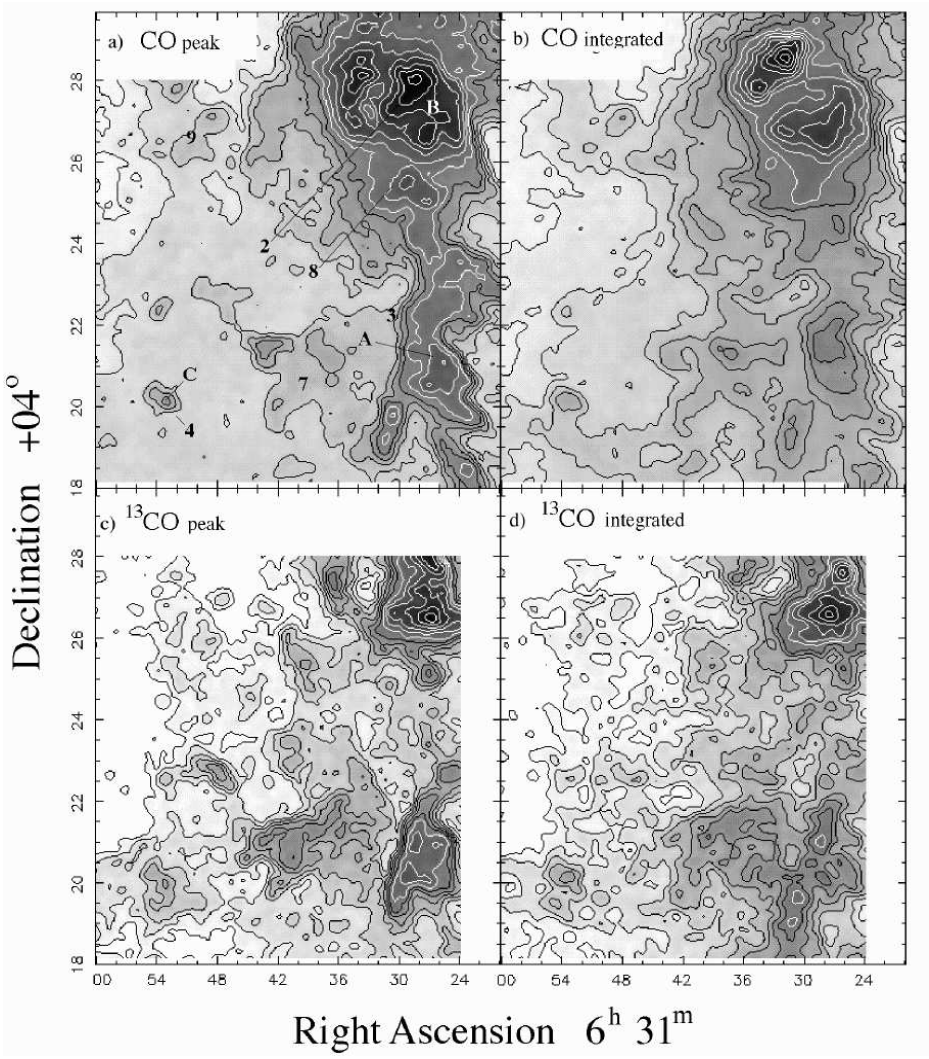

Fig. 1a–d. Maps of the peak and integrated CO and ^{13}CO $J = 2 - 1$ emission from the IRS field. The first contour, and contour intervals for the maps are: **a** (1.5, 2.0) K, **b** (0, 10) K km s^{-1}, **c** (1,1) K, **d** (3,3) K km s^{-1} respectively. The locations of IRAS sources are marked: A is IRAS 06314+0421, B is IRAS 06314+0427 and C is IRAS 06318+0420 and the locations of the globules identified by Patel et al.(1993) are shown, using their numbering system.

H_α filter centred at 656.7 nm, giving an unvignetted field of view of 3′ . The seeing was 0.75″ . These data were calibrated against the white dwarf standard star G193-74 (Oke 1990) observed at a similar airmass.

3. The data

A field which included IRAS 06314+0427, IRAS 06314+0421 and IRAS 06318+0420, and several other globules from the list of Patel et al.(1993) was observed in the CO and ^{13}CO $J = 2-1$ lines. Maps of the peak and integrated emission are shown in Fig. 1.

The CO maps are dominated by emission from an intense region in the NW of the map, centred close to the position of IRAS 06314+0427, and a narrow ridge running to the south for $\sim$ 5 pc. The brightest CO emission in the northern NW is distributed in a broken shell structure, particularly clearly visible in Fig. 1a and b. The ridge is not clearly seen in the ^{13}CO map, which shows a number of clumpy regions along the ridge. Summing the ^{13}CO emission from the ridge, which lies mostly between 14 and 18 km s^{-1}, the mass of material associated with the shell-like source and the ridge is $\sim$ 330 $M_\odot$, for an average kinetic temperature of 15 K, and assuming the line of sight thickness is similar to the projected width.

IRAS 06318+0420 (the second most luminous IRAS source in the area) is clearly identifiable with a rather prominent compact CO and ^{13}CO clump in the SE corner of Fig. 1. IRAS 06314+0427 is associated with the SW rim of the shell-like source. A third IRAS source, IRAS 06314+0421, lies at the centre of a peak in the NS ridge, which is seen prominently in the ^{13}CO map.

Patel et al.(1993) have discussed the possibility that the region close to their Globule 9, may be an area where shock-heating is occurring in the gas, leading to a prominent blue-shifted CO $J = 1 - 0$ wing, without a ^{13}CO counterpart. They reached this conclusion on the basis of the failure to detect ^{13}CO emission at positions where the CO was relatively intense. Careful inspection of the CO and ^{13}CO $J = 2 - 1$ profiles did in fact reveal weak ^{13}CO emission, and the profiles do not appear particularly different from those seen in maps of other quiescent dark clouds. There does not appear to be a need to invoke shock models on the basis of the present data set. It remains somewhat

Fig. 2. The NOT H_α image of Globule 1. The faintest stars visible in this image correspond to $\sim$ magnitude 22. There is noticeable limb-brightening at the N and NW edges of the globule, along the edge facing towards the illuminating stars of the Rosette Nebula. North is at the top, east is to the left.

puzzling why the $J = 1 - 0$ ^{13}CO lines were not detected, although this may be related to their sensitivity and relatively large beam.

Although there is emission in the CO and ^{13}CO maps from the vicinity of Globules 7 – 9 of Patel et al.(1993) (and indicated on Fig. 1), they are clearly not as distinctly recognisable as Globule 1 of Patel et al.(1993), which is relatively isolated from the rest of the cloud material. Fig. 2 shows the narrow band H_α image obtained at the NOT of Globule 1, and the rest of this paper will focus on this object.

Globule 1 has a pronounced head-tail structure. The tail is bifurcated and can be traced for at least 2 arc minutes east of the head — in the direction pointing away from IRAS 06314+0427 — which lies $\sim$ 1.2 pc to the west. A rim of optical emission can be seen surrounding the north west edge of the head, along the edge facing towards the ionising stars of the Rosette Nebula (which lie at position angle 315 degrees (measured from north through east). The lack of visible emission from the rim on the blue POSS plate, and the relatively strong H_α emission on the NOT image implies that the rim has resulted from photoionisation of the outer layers of the globule, rather than being due to scattered light.

Maps showing the integrated CO emission in the CO, ^{13}CO and C^{18}O $J = 2 - 1$ lines, the peak CO $J = 2 - 1$ temperature distribution, and the integrated CO $J = 4 - 3$ line emission are presented in Fig. 3a. The integrated CO map in Fig. 3a shows a similar head-tail structure to the optical image. The centre of the head (at offset (−85,−25) arc seconds) is unresolved in the east-

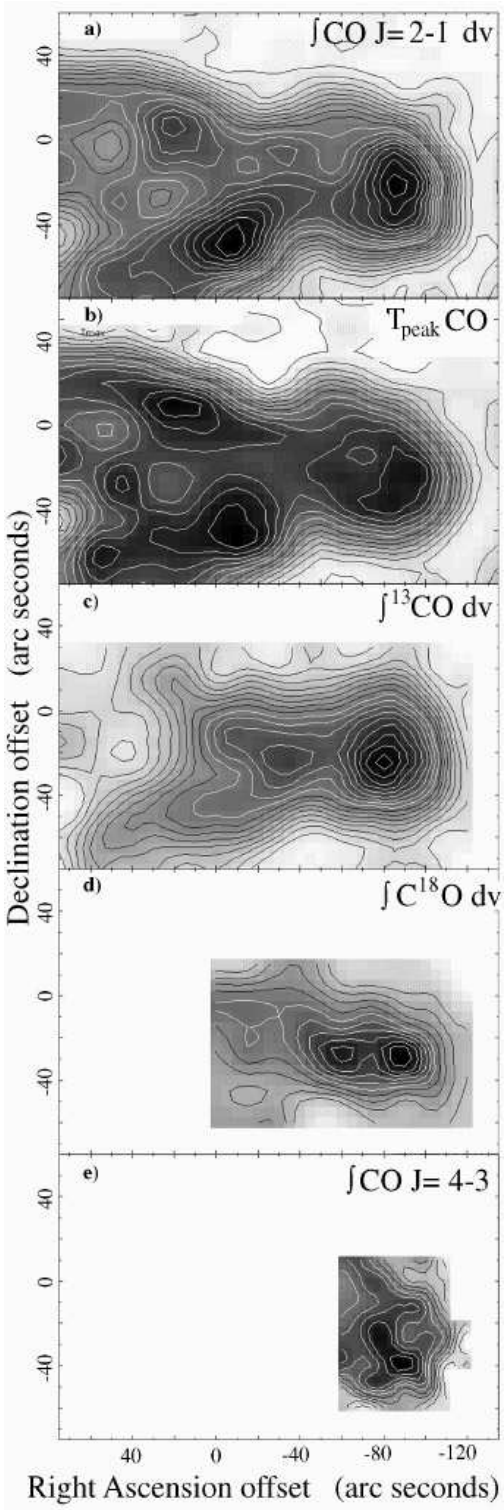

Fig. 3a–e. Maps of **a** integrated CO $J = 2 - 1$ (shown as contours with the first white contour at $T_r{}^* = 2$ K km s^{-1} and contour intervals at 2 K km s^{-1}), **b** peak CO $J = 2 - 1$ $T_r{}^*$ in degrees K, **c** integrated ^{13}CO $J = 2 - 1$ (1, 1 K km s^{-1}), **d** integrated C^{18}O $J = 2 - 1$ (0.5, 0.5 K km s^{-1} and **e** integrated CO $J = 4 - 3$ (28, 4.6 K km s^{-1}).The (0,0) position for the maps of Globule 1 was at $\alpha_{1950} = 06^h\ 32^m\ 19.0^s$, $\delta_{1950} = +04°28'\ 9''$.

west direction but is clearly elongated along a north-south line. Emission along the edges of the tail can also be seen tracing the dark structures visible on the NOT image, with two prominent CO clumps at offsets (−10, −50) and (+20, +10). The globule is sharply bounded to the north, south and west, but CO emission extends beyond the eastern edge of Fig. 3a for $\sim 5'$ (Patel et al. 1993).

The peak values of $T_r{}^*$ in the $J = 2 - 1$ line shown in Fig. 3b are typically $\sim 12 - 14$ K, with the maximum temperatures occurring towards the front of the head, and along the sides of the tail. Since the CO emission is slightly extended compared to the beamwidth, it is appropriate to adopt an efficiency factor somewhere between η_{mb} and η_{fss} (see for example White et al.1986), and the best estimate for the gas kinetic temperature in Globule 1 is ~ 15 K, in good agreement with the FCRAO $J = 1-0$ results of Patel et al.(1993). The sharp decrease of the CO intensities to the north, south and west of the map, suggests there is an abrupt boundary at the edge of the globule.

The ^{13}CO $J = 2 - 1$ map shown in Fig. 3c has a more centrally condensed head than is seen in the CO data, and peaks ~ 10 arc seconds E of the CO peak. The integrated C^{18}O $J = 2 - 1$ emission shown in Fig. 3d has an elongated double core, which is more compact than the CO or ^{13}CO core. A composite diagram showing the relative distributions of the CO, ^{13}CO and C^{18}O $J = 2 - 1$ emission is shown in Fig. 4.

The CO $J = 4-3$ emission integrated over a 1 km s^{-1} wide velocity interval centred on the peak velocity of the CO and isotopomeric lines at 8.5 km s^{-1} is shown superimposed on the $J = 2 - 1$ contours in Fig. 4a. The emission forms a thin shell (width less than 10 arc seconds or 0.08 pc) around the core of the globule. However, this shell is not clearly seen after convolving the $J = 4 - 3$ data to the same resolution as the $J = 2 - 1$ map, and so we are unable to confirm that this shell is made up of warmer gas, which might for example be revealed if the CO $J = 4 - 3$ / $J = 2 - 1$ ratio was ≥ 1. LL95 and González-Alfonso et al.(1995) have noted other examples where there is evidence for warm gas at the outer edges of globules studied by them.

Comparing Fig. 4a-c, the positions of the peaks seen in the different isotopic tracers are slightly displaced from each other, with ^{13}CO $J = 2 - 1$ peaking further away from the edge of the head. In Fig. 4c the C^{18}O $J = 2 - 1$ emission is strongest in a core (~ 30 x 20 arc seconds half-width) elongated along the axis of the globule, and more centrally condensed than either the CO or ^{13}CO distributions, which follow the structure of the dark regions seen in Fig. 2 more closely.

The CO, ^{13}CO and C ^{18}O $J = 2 - 1$ and CO $J = 4 - 3$ channel maps, integrated in 0.5 km s^{-1} intervals are shown in Fig. 5a-d respectively.

The CO map in Fig. 5a exhibits a prominent head-tail structure. Emission from the head peaks close to 8.5 km s^{-1} and extends across the velocity range $6 - 11.5$ km s^{-1}, with broad lines visible towards the leading edge of the head at (−90,−25). In Fig. 5b the ^{13}CO emission has a similar head/split-tail appearance as the CO lines show, although it is more centrally condensed. The C^{18}O emission in Fig. 5c is more localised

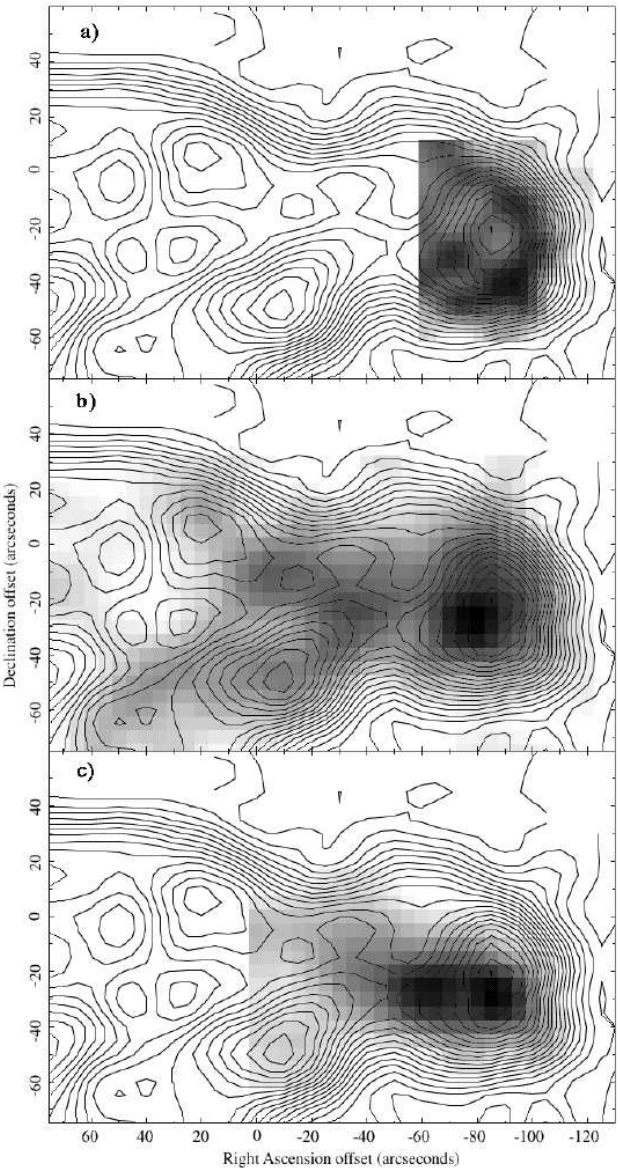

Fig. 4a–c. Comparison of the CO $J = 2 - 1$ integrated emission (shown in each panel as contours) with **a** CO $J = 4 - 3$ emission in a 1 km s^{-1} wide strip centred at + 8.5 km s^{-1}, **b** the integrated ^{13}CO emission and **c** the integrated C^{18}O $J = 2 - 1$ emission. Note that the beam sizes are similar except for the CO $J = 4 - 3$ map shown in **a**.

along the axis - and the double head structure is clearly seen in Fig. 4c. Material in the tail is red shifted (in the south) or blue shifted (in the north) relative to the central velocity of the head. The tail contains a number of peaks which are increasingly red or blue shifted with distance away from the core. This is shown more clearly in Fig. 6 as a position-velocity map along the major axis of the globule.

Fig. 6a shows that the head of the globule between RA offsets −50 and −100 arc seconds has an average velocity of 8.7 km s^{-1}. Further towards the tail, the CO becomes more blue-shifted, characterised by a velocity gradient of 1.4 km s^{-1} pc^{-1}. The CO line is broadened at the front of the head, with low level

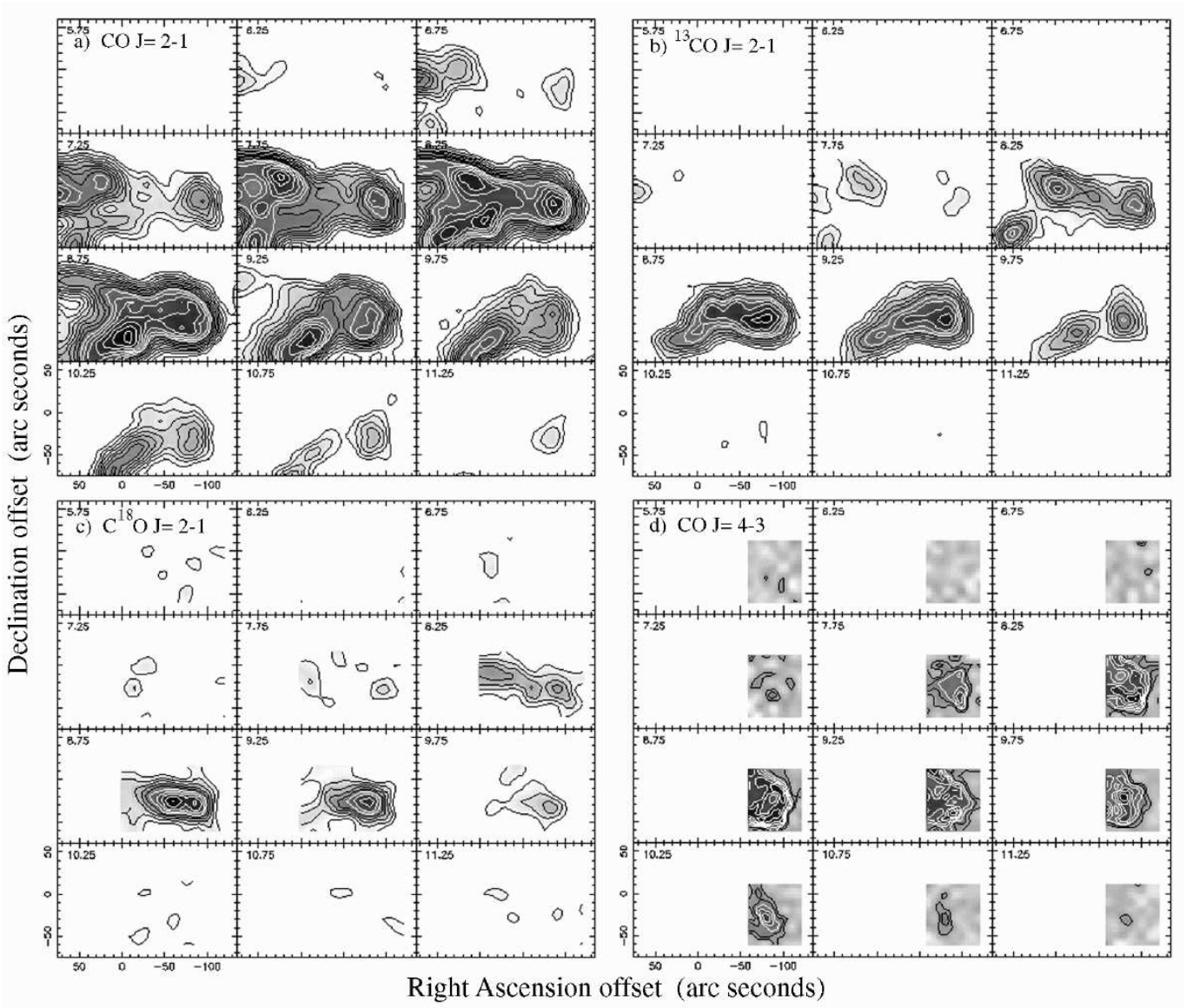

Fig. 5a–d. Channel maps at 0.5 km s^{-1} intervals for **a** CO $J = 2 - 1$ (with the first white contour at 4.7 K km s^{-1} and contour intervals at 0.9 K km s^{-1}), **b** ^{13}CO $J = 2 - 1$ (3.4, 0.43 K km s^{-1}), **c** CO $J = 2 - 1$ (1.2, 0.2 K km s^{-1}) and **d** CO $J = 4 - 3$ (4, 1 K km s^{-1}.)

emission extending between ~ 6 and 12 km s^{-1}, and the CO line centres at the leading edge are slightly blue-shifted by ~ 0.5 km s^{-1} relative to other material in the centre of the head. Faint high velocity wings at the edges of the CO lines are emitted from areas with a similar spatial width as the main body of Globule 1, giving support to a physical association. The chance superposition of an unconnected line-of-sight gas clump is thus unlikely. Bipolar outflows are one of the most frequent explanations for small-scale variations in the kinematics of molecular gas. It may however be difficult (although not impossible) to think of these wings as being due to a bipolar outflow. The small extent of the emitting area might suggest that any outflow is almost perpendicular to the plane of the sky, and while this geometry is the most favourable for detecting high velocity wings, the measured velocity widths seem to be small in comparison with many other outflows in low mass star forming regions to give the idea of an outflow much credence. If this possibility is ruled out, then it appears that the material may be dynamically interacting with ionised gas on the outer surface of the globule, where an ionisation shock front will act on the neutral gas. Similar examples of blue-shifted material close to the heads of other globules have been reported by LL95 and González-Alfonso et al.(1995). The line broadening and velocity shift in Globule 1 are also independently seen in the higher resolution CO $J = 4 - 3$ data shown in Fig. 6c. Across the tail's minor axis, there is a velocity shift of ~ 0.5 km s^{-1}, visible in Fig. 6a.

Spectra taken in various lines in the core of the globule are shown in Fig. 7.

The CO $J = 2 - 1$ and $J = 4 - 3$ spectra shown in Fig. 7 have similar main beam brightness temperatures and central

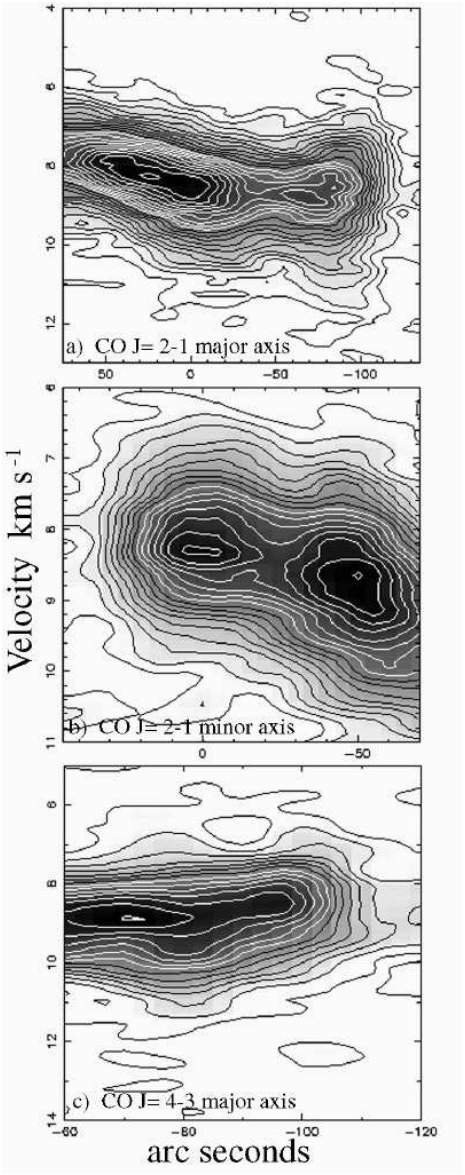

Fig. 6a–c. Position-velocity maps **a** along the major axis of Globule 1 (integrating across an 80 arc second wide strip along the RA axis, centred at Declination offset = −20 arc seconds) in the CO $J = 2 - 1$ line, **b** across the minor axis integrating between RA offsets +20 and -10", and **c** along the major axis in the CO $J = 4 - 3$ line. The first white contour, and the contour intervals (in K km s^{-1}) are respectively **a** (6.4, 0.4), **b** (7.7, 0.8) and **c** (8.4, 0.4).

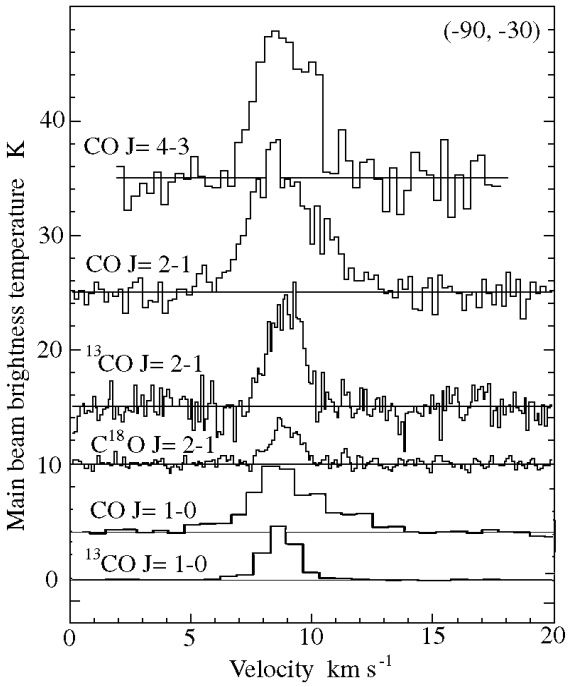

Fig. 7. Spectra in various lines at the offset position (−90, −30) in the globule's head. These spectra are all calibrated in units of main beam brightness temperature, with the $J = 4 - 3$ data convolved to the same beamsize as the $J = 2 - 1$ spectrum to facilitate direct comparison.

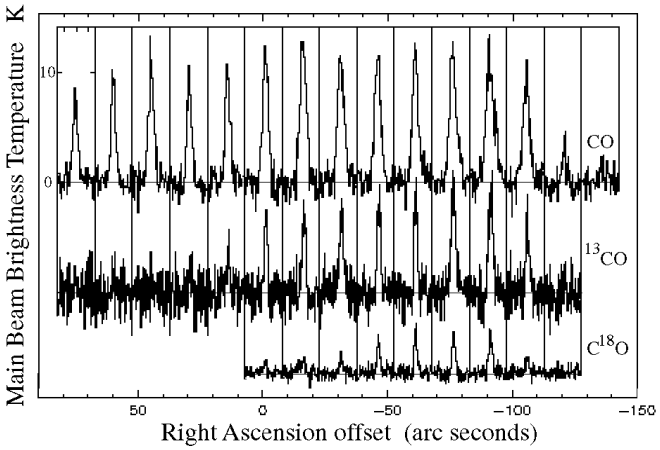

Fig. 8. Montage of spectra of CO $J = 2 - 1$ lines and isotopomers along a strip down the major axis of the globule. All of these spectra are calibrated in main beam brightness temperature units, and plotted to the same scale (which is indicated next to the CO spectra).

velocities. Similarly the CO and ^{13}CO $J = 1 - 0$ OSO spectra have almost identical peak intensities, indicating a kinetic temperature of ~ 10 K. This is slightly lower than indicated by the higher rotational lines, suggesting that the CO emitting region is somewhat beam-diluted with the larger OSO beam. Both the CO and ^{13}CO $J = 1 - 0$ spectra have low level wings which extend from 5 to at least 11 km s^{-1}, a similar velocity range to that seen in the CO $J = 2 - 1$ line.

In Fig. 8, strips of CO, ^{13}CO and C^{18}O $J = 2 - 1$ spectra along the major axis of the globule are shown to illustrate the variation of peak temperatures in the various CO isotopomers.

The $J = 1 - 0$ and $J = 2 - 1$ CO and ^{13}CO line temperatures at the head of the globule are very similar, suggesting extremely high ^{13}CO opacity and / or column density. Similar characteristics were noted in the lower resolution FCRAO $J = 1 - 0$ data of Patel et al.(1993).

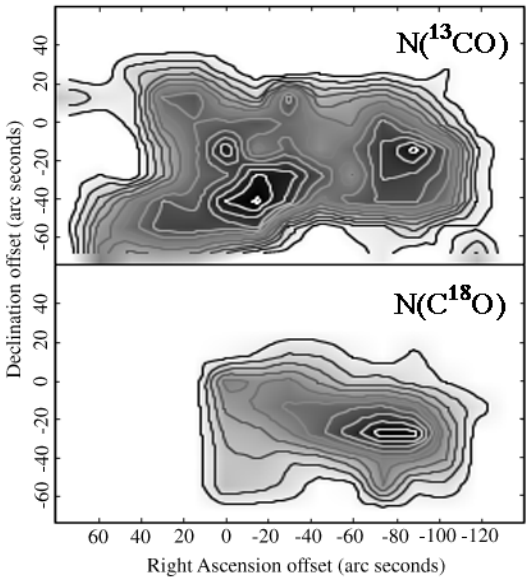

Fig. 9. ^{13}CO and C^{18}O column density maps. The first contour and contour intervals are 2 10^{14} and 2 10^{14} cm^{-2} respectively for ^{13}CO and 1 10^{14} and 1 10^{14} cm^{-2} for C^{18}O - where a standard partition function has been used to estimate the total column density.

4. Analysis

The ^{13}CO and C^{18}O data can be analysed using the LTE approximation to estimate column densities and lower limits to the globule's mass (see White & Sandell 1995, White et al.(1995) for further discussion of the use of LTE effects applied to column density determination). Maps of the ^{13}CO and C^{18}O column densities derived in this way are shown in Fig. 9.

The C^{18}O column density peaks further into the body of the globule than the leading edge of the CO in the head (see Fig. 3), suggesting that the denser core is surrounded by a sheath of lower column density material. In view of the relatively high opacities implied by the strength of the CO isotopes, the possibility of self-absorption on the CO lines should not be ignored, although there is little evidence of narrow self-absorption features amongst any of the spectra in the mapped region.

The mass of the Globule 1's core, M_c, was estimated separately using the ^{13}CO and C^{18}O $J = 2 - 1$ lines, adopting canonical abundance ratios of [CO]/[^{13}CO] = 67, [CO]/[C^{18}O] = 500 and [CO]/[H$_2$] = 8 10^{-5}. The derived values of M_c were similar: 16 $M_\odot$ from the C^{18}O data and 15 $M_\odot$ from the ^{13}CO data. These values are almost an order of magnitude lower than that originally estimated by Patel et al.(1993) for Globule 1 - primarily because the size of the globule that they assumed was too large. Taking the C^{18}O data, and assuming that the depth of the globule perpendicular to the plane of the sky is similar to it's projected width, the mean particle density is $n_{H_2} \sim 5500$ cm^{-3}.

Since ^{13}CO is an unreliable estimator of column density in the denser parts of cloud cores (White & Sandell 1995), it is somewhat surprising that the cloud mass estimates made from the ^{13}CO and C^{18}O data sets are so similar. Although estimates of masses from ^{13}CO data almost certainly underestimate the column density (and hence the mass) in the head, it does sample material over a more widespread area of the tail than the C^{18}O data traces. A separate estimate of the most likely cloud mass was then made by using the C^{18}O data to determine the column densities in the core, the ^{13}CO data for the tail behind the head, and the CO data at the eastern edge of the tail where the ^{13}CO emission is too weak to detect. In the latter case we have followed the technique outlined by González-Alfonso et al.(1995) using the conversion;

$$N(H_2) = [0.5 + 0.2W(CO)]\ 10^{21} cm^{-2} \quad (1)$$

where *W(CO)* is the integrated CO intensity in K km s^{-1}, based on the work of Cernicharo & Guélin (1987). To first order, we estimate with the simplest assumptions about the 3-dimensional geometry, that the lower limit to the mass of the globule is 25 $M_\odot$, made up by 20 $M_\odot$ in the head, and 5 $M_\odot$ in the tail.

To check whether the core of Globule 1 is gravitationally bound, the core mass can be compared with its Virial Mass, M_{vir}. Using the average C^{18}O line width of 1.1 km s^{-1}, a radius of 0.18 pc, and assuming density laws which scale as $n \propto$ r, r^{-1} or r^{-2}, the virial mass is 42, 39, or 25 $M_\odot$ respectively (see MacLaren et al.1988). Since $M_{vir} > M_c$, the cloud does not appear to be gravitationally bound. It is however possible that the effects of opacity, magnetic fields, turbulence, shocks and the non-sphericity of the core will all conspire in such a way that the M_{vir} may have been over-estimated; given these uncertainties there is no compelling reason to believe that Globule 1 is other than gravitationally bound. The gravitational stability of globules has been examined by LL94, who show that although the globules will be bounded by self-gravity and the pressure of out-flowing ionised gas, there may still be a requirement for additional magnetic support if they are to be stable. Patel et al. (1993) have drawn similar conclusions, deducing that although Globule 1 may at best be critically self-bound, the presence of the IRAS source in the head suggests that collapse has already taken place, perhaps initiated by a radiation-driven implosion.

To understand the ratios of the CO/^{13}CO peak temperatures, which are close to unity, the observed $J = 1 - 0$ and $J = 2 - 1$ CO/^{13}CO antenna temperatures were compared with the predictions of an LVG model. This calculation was carried out for a kinetic temperature = 15 K. The $J = 1 - 0$ data were taken from Fig. 5 of Patel et al.(1993), and the $J = 2 - 1$ data were obtained by smoothing the JCMT data to the same resolution as the FCRAO data. A χ^2 fit was made to the $J = 1 - 0$ and $J = 2 - 1$ line ratios at two positions; (-40, -20 at the centre of the head) with a best fit column density (N(H$_2$) / $^{dv}/_{dr}$) = 3 10^{17} cm^{-2} km^{-1} s, and volume density n_{H_2} = 2 10^4 cm^{-3}; and (-70, -20 at the front of the head) where the column density (N(H$_2$)/$^{dv}/_{dr}$) = 3 10^{18} cm^{-2} km^{-1} s and volume density n_{H_2} = 4 10^3 cm^{-3}. These LVG column densities are almost an order of magnitude greater than values estimated from the ^{13}CO data using the LTE method (with a first order opacity correction), but agree to within a factor of ~ 2 with the CO column density

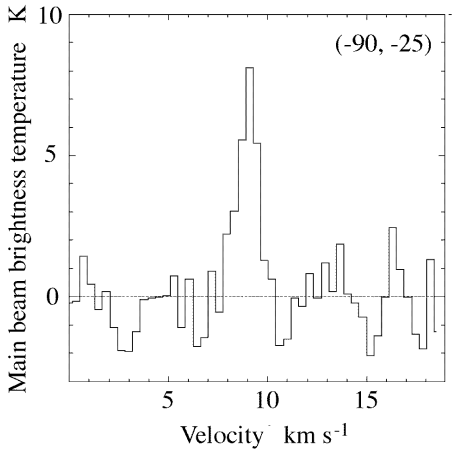

Fig. 10. CI spectrum at the offset position (−90, −25), close to the centre of the head. This spectrum is calibrated in main beam brightness temperature.

inferred from $C^{18}O$, and those estimated from CS observations by Patel et al.(1993) towards the centre of the head.

To further examine the effect of the external UV radiation field on material associated with Globule 1, we obtained a single $^3P_1 - {}^3P_0$ CI spectrum towards the head, which is shown in Fig. 10. White & Sandell (1995) and Minchin et al.(1995 a,b) have recently shown that the abundance ratio [CI]/[CO] in ultra violet irradiated regions is correlated with the $C^{18}O$ column density and hence with the (presumed) UV radiation field. Relatively high values of [CI]/[CO] might therefore be expected towards an object such as Globule 1.

The CI spectrum has a single peak centred at 9.0 km s^{-1}, with a line width of 1.2 km s^{-1}, similar to that seen in the $J = 2 - 1$ $C^{18}O$ line, and an integrated main beam brightness temperature = 10.7 K km s^{-1}. The LTE column density (assuming optically thin conditions and that the excitation temperature is similar to that of CO (Padman et al.1996)) is $\sim 4\ 10^{17}$ cm^{-2}. The beam averaged CO column density (estimated from the optically thin(ner) $C^{18}O$ line) at this point is $7.5\ 10^{17}$ cm^{-2}, which implies [CI]/[CO] 0.5±0.06. This ratio is at the high end of the [CI]/[CO] ratios observed in the vicinity of the high UV environment near the Orion Nebula and Bright Bar ionisation front, where [CI]/[CO] varies between $\sim$ 0.05 and 0.3 (White & Padman 1991). High [CI]/[CO] have recently been observed towards a low extinction high galactic latitude cloud by Stark & van Dishoeck (1994) and in the highly photoionised gas of the starburst galaxies M82 and NGC 253 (White et al.1994, Israel et al.1995). The relatively high value of [CI]/[CO] is consistent with the trends which have recently been proposed connecting CI and CO column densities in other photoionised sources, and future observations of the CI distribution may be a good probe of material close to the globule's outer photodissociated edge.

The UKIRT 2.122 μm H_2 S(1) line image is shown in Fig. 11a. An additional frame taken in the 2.166 μm Brackett-γ (hereafter Br_γ) line suffered from uncertain flat-fielding, but there does not appear to be any Br_γ emission with a flux > 5

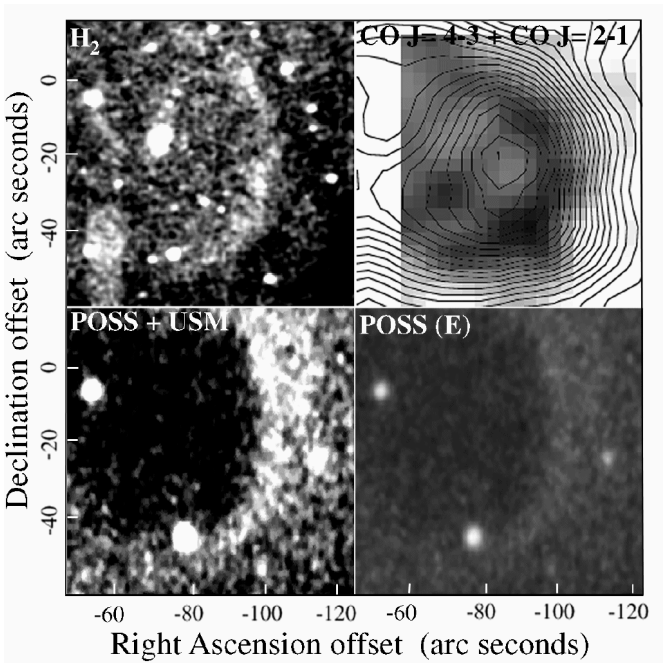

Fig. 11. a UKIRT H_2 v=1-0 S(1) image at 2.122 μm ; the peak intensity of the diffuse emission on the leading edge of the globule has a peak value of 6.4 10^{-14} W cm^{-2} sr^{-1}, **b** CO $J = 4 - 3$ emission at +8.5 km s^{-1} overlaid with contours of the integrated CO $J = 2 - 1$ emission, **c** contrast enhanced POSS red image and **d** POSS red image digitised directly from a glass plate copy (without subesquent contrast enhancement).

10^{-15} W cm^{-2} sr^{-1} (or more than about 10 percent of the peak H_2 line flux). The H_2 S(1) line shows a thin rim of emission surrounding the leading edge of the head, at a similar location as the CO $J = 4 - 3$ gas at 8.5 km s^{-1} shown in Fig. 11b. There is also some diffuse low level H_2 emission which extends over most of the head of the globule. Optical emission from the rim is also faintly visible on the POSS red plate (Fig. 11d, and more clearly seen on the NOT H_α image in Fig. 2, coincident with the CO $J = 4 - 3$ gas at 8.5 km s^{-1}. By contrast, the CO $J = 2-1$ core lies just inside the optical/H_α rim. The prominent near-infrared object which is inside the head of Globule 1 at offset (−71, −18), is absent from both the H_α and red and blue POSS images, and is a highly reddened object, which is possibly associated with the infrared source IRAS 06322+0427.

The integrated H_2 S(1) flux from the 'arc' feature at the head of Globule 1 is $9.7\ 10^{-5}$ ergs s^{-1} cm^{-2} sr^{-1}. Following the commonly adopted assumption in clouds like this that molecular hydrogen can be characterised by having a rotational temperature of $\sim$ 2000 K (Brand et al.1988, Burton et al.1989, Garden et al.1986), then the H_2 column densities are related to the v = 1-0 S(1) line intensity I_{H_2} by;

$$N(H_2) = 2.93\ 10^{21}\ I_{H_2} \quad cm^{-2} \tag{2}$$

where this equation is obtained by substituting appropriate numerical constants into the relationship of Gautier et al.(1976), and $N(H_2)$ is the number of H_2 molecules cm^{-2}.

Using this relationship, the column density and mass of the molecular hydrogen visible in Fig. 11a are estimated to be 3.0 10^{17} cm^{-2} and 1.5 10^{-4} M$_\odot$ respectively.

Optical emission lines emitted from material at the photodissociated edges of cometary globules should be dominated by hydrogen recombination line emission and moderate excitation states of C, N, O and S. Poglitsch et al.(1995) have shown that the minimum number of Lyman continuum photons required to ionise a region, assuming case B recombination for a 'standard' H II region (electron density = 10^4 cm^{-3} and T$_e$ = 10^4 K), is given by;

$$N_{Ly_c} = \frac{3\ 10^{47}\ L_{Br_\gamma}}{f\ L_\odot} \quad (3)$$

where N_{Ly_c} is the rate of ionising photons (s^{-1}), L$_{Br_\gamma}$ is the Br$_\gamma$ line luminosity and f is the fraction of Lyman photons photo-electrically absorbed.

The upper limit to the Br$_\gamma$ emission emitted from Globule 1 is 1.0 10^{-5} erg s^{-1} cm^{-2} sr^{-1} (averaged over the same area as the H$_2$ rim), corresponding to a flux of 1.2 10^{-13} ergs s^{-1} cm^{-2}. From (3), this implies that the upper limit to any ionising flux $N_{Ly_c} \lesssim 3\ 10^{45}$ s^{-1}. The total Lyman continuum flux illuminating the head of Globule 1 from the Rosette OB cluster is $\sim$ 1.3 10^{45} s^{-1}, and so the Br$_\gamma$ upper limit available from our data is just consistent with that which would be expected as a result of the UV illumination by the Rosette OB star cluster. The ionising flux from IRAS 06314+0427 at the surface of the globule is probably less than that from the OB cluster, since the putative O7 star is almost certainly surrounded by dust.

5. Discussion

The effect of external radiation on a globule has been shown to lead to the Radiation Driven Implosion (RDI) of a cloud, followed by the formation of a dense core extended along the cloud's axis (Sanford et al.1982, 1984). Bertoldi (1989) and Bertoldi & McKee (1990) found that this process occurred in two phases; an early collapse phase as the effect of the ionising radiation compresses and ionises the globule, and a cometary phase in which the external ionised gas shields the tail from ionising radiation and pressure confines the head, leading to a long-lived head-tail morphology. During this latter phase of the globule's evolution, it moves away from the illuminating source at a velocity of $\sim 5 - 10$ km s^{-1}. LL94 and LL95 have developed a more comprehensive model which appears to be very successful in explaining a range of geometrical configurations for cometary globule's which have been observed to date.

The formalism of LL95 has been used to model the observationally constrained characteristics of the head of Globule 1. This is a 2-D hydrodynamical simulation which describes the formation and evolution of a cometary globule as a consequence of a radiatively driven implosion. In this model, the cloud is treated as an isothermal sphere of cold dense gas, surrounded by a hot ambient medium initially in pressure equilibrium. Its evolution is primarily determined by two dimensionless parameters: the ratio of the ionised gas and the initial cloud's densities,

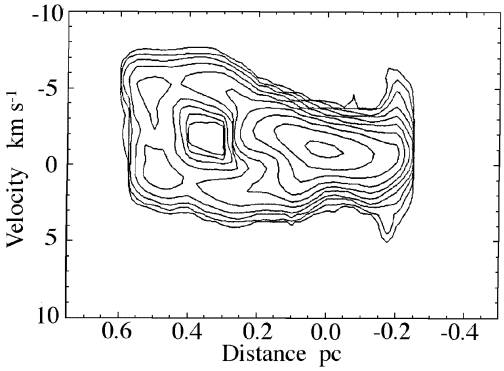

Fig. 12. RDI simulation of the major axis position velocity data shown in Fig. 6a. The model assumes a velocity dispersion of 1.5 km s^{-1}, equivalent to a half-power linewidth of 3.5 km s^{-1} (with a viewing angle of 20 degrees from the normal). The contour levels follow the style of LL94, and are in arbitrary units of density following the relationship $\Delta\ log\ \rho = m/2$, where m is an integer in the range -1 to 4.

and the fraction of UV photons absorbed in a thin ionised boundary layer at the front of the cloud. Additionally the dynamics of gas in the head of the globule will be influenced by the propagation of an isothermal shock. After about 10^5 years, a dense core will be formed inside the head, whilst the compression continues deeper into the cloud, eventually forming small ansae along the major axis of the cloud (*i.e.* aligned with the direction of the illuminating stars responsible for the RDI). At this stage the density contrast between the core and the initial cloud material will be about one order of magnitude. Finally, the cloud enters a quasi-equilibrium state, when the cometary head becomes confined by over-pressure of the ionised gas. The globule, and its now well developed tail structure, will ultimately acquire a bulk velocity away from the external radiation source at velocities of typically $\sim$ 10 km s^{-1}.

Previous results (LL94) showed that the morphological evolution of the cloud was not very sensitive to the ionisation parameters. We selected model 2 of LL94 for its evolutionary stage, by looking for the best kinematical and morphological match with the observations. Note that in our simulation, we adopt a planar illumination, perpendicular to the cloud's major axis. This means that we neglect any possible influence of the UV flux from the Rosette Nebula when comparing the results with Globule 1 (this point is discussed further below). To facilitate comparison between the simulations and the data, we scaled the numerical results to match the radii of the simulated globule and of Globule 1 (see LL94).

In Fig. 12, the RDI model prediction is shown, which should be compared with the observational position velocity diagram in Fig. 6a.

Rather than calculating a series of velocity-channel maps which attempt to match all of the details of the gas kinematics, we found it more interesting to simulate the on-axis position velocity diagram. We have integrated this across the globule's width to lay stress on the main kinematical features, rather than try to model every small detail of the kinematics. The RDI model

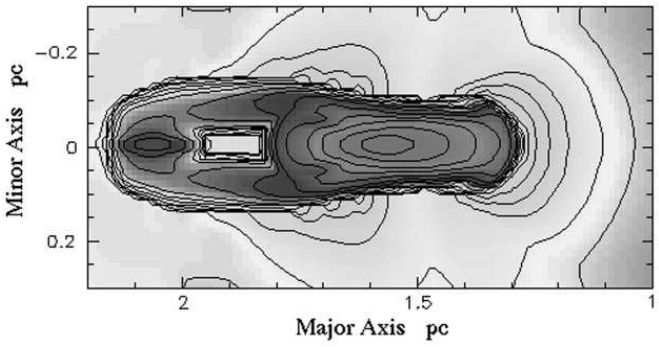

Fig. 13. Simulated density distribution of the globule. The contour levels are in arbitrary units following the style of LL94. In this context the comparison of the general shape of this simulated density plot with the column density plots shown in Fig. 9 is more important than matching the exact column or volume densities, which are model and geometry dependent.

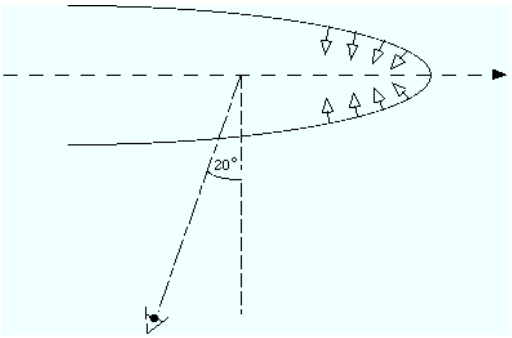

Fig. 14. Geometry of the globule

Table 2. Comparison between the RDI model and Globule 1

Property	RDI Simulation	Globule 1
Mass $M_\odot$	49	25 - 42
Core radius (pc)	0.18	0.18
Age (years)	400,000	700,000
Vel grad (km s^{-1} pc)	2.2	1.4
UV flux (cm^{-2} s^{-1})	1.1 10^9	9 10^8

successfully simulates the large velocity gradient in the main body of the globule, as well as recovering the kinematics of the blue and red wings. The characteristics of the simulated globule are compared with the observed characteristics inferred for Globule 1 in Table 1, in which we have adopted a value for the illuminating flux from Patel et al.(1993).

Fig. 13 shows how the simulated column density distribution follows the observed distribution, as well as reproducing the bifurcated tail structure and dense core elongated along the major axis - as seen in the data shown in Fig. 3.

There is thus reasonably good agreement between the model predictions and the observed characteristics of Globule 1. The simulation suggests that Globule 1 has nearly reached the maximum compression stage following the initial collapse phase, just prior to entering the quasi-static cometary phase.

The model used in this paper is based on the simplest hypothesis; the description of the finer details seen in the observations would have been at the cost of making assumptions about many more parameters (such as the initial density profile), and therefore might have appeared less convincing in this respect. It is no wonder that the model fails to reproduce some of the kinematic features of Globule 1 — as mentioned above, our boundary conditions are different for the UV flux, since we cannot accurately take into account the illumination from the Rosette Nebula stars, although these must these have an effect on the evolution of the globule, as can be seen from Fig. 2. The sign of the velocity gradient in the tail suggests that the head of the globule points out of the plane of the sky at an angle of ~ 20 degrees — explaining why the blue wing is seen to be slightly ahead of the redshifted component, as was indicated in Fig. 12. The proposed geometry is sketched in Fig. 14.

The differences between the velocity gradient predicted by the model and that observed in the data, and in the shape of the observed/simulated tail are the likely consequences of simplifications in our model. In particular, the observed 'bending' of the redshifted tail component and the 'hole' produced in the faintest part of the tail of the simulated cloud are not simultaneously matched to the data and simulation. Nevertheless, the relatively good agreement between the other observations and the simulation suggests either that the globule has rotated significantly after the initiation of RDI, or more likely that the collapse is being influenced by one or more of the nearby IRAS sources.

It is not clear how the bulk velocity of the ambient material in Globule 1 is related to the larger scale kinematics of the surrounding gas. Blitz & Stark (1986) averaged together ~ 3000 ^{13}CO spectra of the Rosette Molecular Cloud, finding gas velocities ranging from $11-16$ km s^{-1}. The ^{13}CO maps of Blitz & Thaddeus (1980) indicated that the mean velocity of the *extended* gas near to the globule has a similar range to that found by Blitz and Stark (1986), meaning that Globule 1 has a mean velocity difference of $\sim 2-7$ km s^{-1} relative to nearby (*i.e.* line of sight or background) gas. Velocity differences of this magnitude are similar to those modelled by Bertoldi & McKee (1990) and LL94 for cometary globules in the pre-cometary phase at an age of $\sim$ 200,000 years.

Patel et al. (1993) have noted that the column densities and ionising flux at the surface of Globule 1 are well described by the Bertoldi (1989) model, for a cloud which is compressed by an ionisation front-driven shock, with a thin external ionisation boundary layer around the head. Our derived column densities are similar to those estimated by Patel et al.(1993), and support their general conclusions. The present results do however go much further in suggesting the presence of excited material around the leading edge of the globule The most likely explanation of this is that it lies close to the ionised boundary layer, and may trace the precursor shock to the ionisation front.

6. Summary

1. Globule 1 has a well-developed head-tail structure, with a head of diameter ~ 0.4 pc, and a tail extending at least 1.3 pc behind it. The major axis of the globule points about 45 degrees away from the direction of the (presumed) illuminating stars at the central of the Rosette Nebula, and ~ 20 degrees from the plane of the sky as we view it. The globule's major axis currently points in the general direction of the luminous infrared source IRAS 06314+0427, but it remains unclear whether this has affected the evolution significantly.
2. The CO lines are broadened at the front of the head of Globule 1, and there is a velocity gradient ~ 1.4 km s^{-1} along the tail. The velocities of gas at the front of the head are blue-shifted by ~ 0.5 km s^{-1} compared to the rest of the material in the head.
3. The CO $J = 2 - 1$ temperature peaks towards the front of the globule's head, and along the edges of the tail, while the molecular column densities peak at the front of the head, and along the southern edge of the tail. The ^{13}CO $J = 1 - 0$ and $J = 2 - 1$ line temperatures in the head are similar to those of their CO counterparts, suggesting very high opacities or column densities. There is a narrow rim of CO emission visible in the higher spatial resolution $J = 4-3$ data at 8.5 km s^{-1} around the front of the head. This shows some correlation with an optical rim, and narrow ridge of molecular hydrogen emission with a column density $3\ 10^{17}$ cm^{-2} and mass $\sim 1.5\ 10^{-4}$ M$_\odot$. An unsuccessful search for Br$_\gamma$ emission gave upper limits just above that expected if the primary illuminating source is the Rosette OB star cluster.
4. The data give strong support to the RDI model and the model of LL94. The simulation carried out in this paper has been able to produce a remarkably good fit to the observed general morphological structure, including the relative CO, ^{13}CO and C^{18}O distributions, and the kinematics of the gas. The globule appears to have an age $\sim$ 400,000 years, a mass $\sim$ 50 M$_\odot$ and has almost reached the stage of maximum compression — and is about to enter the quasi-static cometary phase of it's evolution
5. Observations of the molecular cloud to the west of Globule 1 reveal a complex structure with material mostly lying on a clumpy ridge running NS, with a bright shell-like CO source at the northern end — the total masses of this source and the ridge are ~ 330 M$_\odot$. There are ^{13}CO peaks associated with each of the IRAS sources in the mapped area, but the identification of some previously catalogued Globules is less clear.

Acknowledgements. We thank the UK Science & Engineering Research Council for supporting the Submillimetre Wave Astronomy and Instrumentation programme at QMW and providing travel funds. The JCMT and UKIRT are operated by the Royal Observatory, Edinburgh on behalf of the UK Particle Physics and Astronomy Research Council, The Netherlands Organisation for Scientific Research and the Canadian National Research Council. The UKIRT is operated by the Royal Observatory, Edinburgh. We thank the Onsala and Nordic Optical Telescope staffs for operation of the OSO 20 metre and NOT 2.5 m telescopes respectively; The Royal Society for providing funding from their Research Grant Scheme which allowed the purchase of Image Processing Equipment needed for the data analysis; Dr Mike Irwin of the RGO for digitising the POSS glass plates of the area around the Globule 1; Dr Rene Liseau for seeking funding from the Swedish Natural Science Research Council to support the NOT observations; the referee for helpful comments.

References

Bertoldi, F. 1989, ApJ 346, 735
Bertoldi, F., McKee, C.F. 1990, ApJ 354, 529
Blitz, L., Thaddeus, P. 1980, ApJ 241, 676
Blitz, L., Stark, A.A. A&A. 1986, ApJ 300, L89
Block, D.L. 1990, Nature 347, 1990
Block, D.L., Dyson, J.E., Madsen, C. 1992, ApJ 390, L13
Brand, P.W.J.L., Moorhouse, A., Burton, M.G. et al., 1988, ApJ 334, L103
Burton, M.G., Geballe, T.R., Brand, P.W.J.L. 1989, MNRAS 238, 1513
Cernicharo, J., Guélin, M. 1987, A&A 176, 299
Cox, P., Deharveng, L., Leene, A. 1990, A&A 230, 181
Dorland, H., Montmerle, T., Doom, C. 1986, A&A 160, 1
Ellison, B.N., Claude, S.X.M., Jones, A., Matheson, D.N., Little, L.T. , Davies, S.R. 1996 Digest International Conference on Mm and Submm Waves and applications, in press
Hawarden, T.G., Brand, P.W.J.L. 1976, MNRAS 175, 19
Garden, R., Geballe, T.R., Gatley, I., Nadeau, D. 1986, MNRAS 220, 203
Gautier, T.N., Fink, U., Treffers, R.R., Larson, H.P. 1976, ApJL 207, L129
González-Alfonso, E., Cernicharo, J., Radford, S.J.E. 1995, A&A 293, 493
Israel, F.P., White, G.J., Baas, F. 1995, A&A 302, 343
Lefloch, B., Lazareff, B. 1994, A&A 289, 559 (LL94)
Lefloch, B., Lazareff, B. 1995, A&A 301, 522 (LL95)
MacLaren, I., Richardson, K.M., Wolfendale, A.W. 1988, ApJ 333, 821
Minchin, N., White, G.J., Ward-Thompson, D., 1995a A&A 301, 894
Minchin, N., White, G.J., Ward-Thompson, D., 1995b, A&A 302, L25
Oke, J.B. 1990, AJ 99, 1621
Padman, R., Hobson, M., White, G.J., Pinnock, S. 1996, A&A in press
Patel, N.A., Xie, T., Goldsmith, P.F. 1993, ApJ 413, 593
Poglitsch, A., Krabbe, A., Madden, S.C. et al., 1995, MPE preprint 310
Reipurth, B. 1983, A&A 117, 183
Sanford, M.T., Whitaker, R.W., Klein, R.I. 1982, ApJ 260, 183
Sanford, M.T., Whitaker, R.W., Klein, R.I. 1984, ApJ 282, 178
Stark, R., van Dishoeck, E.F. 1994, A&A 286, 443
Sugitani, K., Fukui, Y., Ogura, K. 1991, ApJS 77, 59
White, G.J., Avery, L.W., Richardson, K.J., Lesurf, J.C.G., 1986, ApJ 302, 701
White, G.J. 1988, *Millimetre and Submillimetre Astronomy*, ed Wolstencroft, R. and Burton, W.B., D. Reidel Press, p.27-94
White, G.J., Padman, R. 1991, Nature 354, 511
White, G.J. Ellison, B., Claude, S., Dent, W.R.F., Matheson, D.N. 1994, A&A 284, L23
White, G.J. 1994, A&A 274, L33
White, G.J., Casali, M., Eiroa, C. 1995, A&A 298, 594
White, G.J., Sandell, G. 1995, A&A 299, 179

This article was processed by the author using Springer-Verlag LaTeX A&A style file *L-AA* version 3.